The University of Reading

2D advection in an idealised convection model

Debbie Clifford, Sarah L. Dance, Robin J. Hogan

MATHEMATICS REPORT 2/2011

Department of Mathematics and Statistics
The University of Reading
Whiteknights, PO Box 220
Reading
Berkshire RG6 6AX

Department of Mathematics and Statistics

2D advection in an idealised convection model

Debbie Clifford[1], Sarah L. Dance[1,2] and Robin Hogan[1]

[1]National Centre for Earth Observation, Department of Meteorology,
[2]Department of Mathematics and Statistics,

University of Reading, Earley Gate, Reading, RG6 6BB, UK.

d.j.clifford@reading.ac.uk

Feb 2011

Abstract

An idealised 2D convection model is described here, which requires the use of a total variation diminishing (TVD) advection scheme. Two such schemes are tested, but while both are stable in the 1D case, one develops an unusual instability in the 2D case which is not well understood.

1 Introduction

An idealised 2D moist convection model is described here, based on the dry convection model MIDAS, written by Cyril Morcrette (Morcrette and Browning, 2006). This sort of simple model of convection-driven rainfall would allow, for instance, investigation of the assumptions made when assimilating rainfall radar data. MIDAS simulates a two-dimensional cross-section through a front, with one vertical dimension and one horizontal, and the prognostic fields are vorticity, along-front wind and potential temperature, which is a tracer. To extend the model to moist convection and generate rain, new prognostic fields of total water mixing ratio and rainwater mixing ratio are added, and the potential temperature is replaced by the liquid water potential temperature.

Advection in the moist model is problematic. MIDAS uses the Arakawa Jacobian to advect model fields (see for instance Haltiner and Williams (1980)). This scheme is simple to understand and implement, but suffers from some numerical problems, most importantly the introduction of spurious oscillations or ripples in the presence of strong gradients (Peterson and Hammett, 2008). While this is compensated for somewhat by a diffusion term in the model equations, and causes no noticeable problems for a dry scheme, the physical impossibility of negative values in water content fields means a more sophisticated advection scheme is required for the moist model.

To advect these moisture gradients without generating ripples requires a Total Variation Diminishing (TVD) scheme, which prevents any over- or under-shoot in the advected fields. One approach is to use a flux-limiter, a mathematical function that weights the scheme between a high-order to a low-order flux term in the presence of changes in gradient in the advected field. Many choices for this flux-limiting function exist, and there are many ways of formulating an advection scheme around them. As part of this work, a scheme by Kurganov and Tadmor (2000) has been implemented, which demonstrates the interesting behaviour of being stable in 1D, while implementation in 2D generates instabilities that are not fully understood.

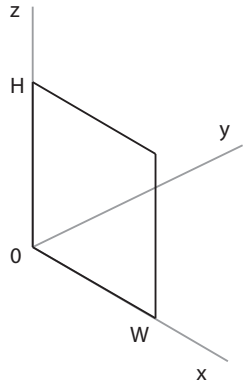

Figure 1: Model domain, shown outlined in black. The domain is a cross-section through an infinite front in the y-direction, with height H and width W.

Section 2 of this report describes the extended, moist version of MIDAS; complete documentation for the model can be found in Clifford (2011). Section 3 introduces the principles for flux-limiting schemes and describes the Kurganov and Tadmor scheme in detail, along with a simpler flux-limiting scheme. Section 4 presents the results of convergence and stability tests for the schemes in 1D, and the results of extending the schemes to 2D.

2 Model description

The model domain is a 2D cross-section through an infinite front, where derivatives in the along-front direction are assumed zero. The cross-frontal direction is x, along-front is y and vertical is z, as shown in figure 1. The prognostic variables in the model are vorticity η, along-front wind v, liquid water potential temperature θ_l (following Tripoli and Cotton (1981) and Sun and Crook (1997)), total water mixing ratio q_t and rainwater mixing ratio q_r. The dynamical equations are set up in vorticity-streamfunction (η-ψ) form, with

$$\nabla^2 \psi = \eta, \tag{1}$$

and the cross-frontal wind u and vertical wind w being, respectively,

$$u = \frac{\partial \psi}{\partial z}, w = -\frac{\partial \psi}{\partial x}. \tag{2}$$

Before convection is initiated the front is in thermal wind balance, where the horizontal derivative in the virtual potential temperature θ_v balances the vertical wind-shear of the along-front wind:

$$f\frac{\partial v}{\partial z} = \frac{g}{\theta_{v0}}\frac{\partial \theta_v'}{\partial x}. \tag{3}$$

g is the acceleration due to gravity and f the Coriolis parameter. Subscript 0 represents a hydrostatic reference state, and primed quantities are departures from this state. The prognostic equations as

solved by the model are:

$$\frac{\partial \eta}{\partial t} + u\frac{\partial \eta}{\partial x} + w\frac{\partial \eta}{\partial z} = f\frac{\partial v}{\partial z} - \frac{g}{\theta_{v0}}\frac{\partial \theta_v'}{\partial x}, \tag{4}$$

$$\frac{\partial v}{\partial t} + u\frac{\partial v}{\partial x} + w\frac{\partial v}{\partial z} = -fu, \tag{5}$$

$$\frac{\partial \theta_l}{\partial t} + u\frac{\partial \theta_l}{\partial x} + w\frac{\partial \theta_l}{\partial z} = -\frac{\theta_l^2}{\theta}\frac{L_{lv}}{C_p T}\frac{Dq_t}{Dt}\Big|_{rain}, \tag{6}$$

$$\frac{\partial q_t}{\partial t} + u\frac{\partial q_t}{\partial x} + w\frac{\partial q_t}{\partial z} = -\text{Autoconversion} - \text{Accretion} + \text{Evaporation}, \tag{7}$$

$$\frac{\partial q_r}{\partial t} + u\frac{\partial q_r}{\partial x} + w\frac{\partial q_r}{\partial z} = +\text{Autoconversion} + \text{Accretion} - \text{Evaporation} - \frac{d(V_{Tm}q_r)}{dz}. \tag{8}$$

$$\tag{9}$$

$Dq_t/Dt|_{\text{rain}}$ is the external derivative of the liquid water content (external to the parcel, i.e. the change in liquid water due to advection/precipitation as opposed to phase changes). θ is the potential temperature, and the thermodynamic parameters are the latent heat of vaporization L_{lv} and the specific heat of water C_p. Other diagnostic quantities in the prognostic equations are the temperature T and the rainwater terminal velocity V_{tm}. The warm rain processes of autoconversion, accretion and evaporation are parameterized following Sundqvist (1978) and Wilson and Ballard (1999), and will not be defined further here - see the model documentation (Clifford, 2011) for further details. Both boundaries in the horizontal direction are periodic:

$$\xi\left(0, z\right) = \xi\left(L, z\right). \tag{10}$$

Vertical velocities are zero at the top and bottom of the domain, the no normal flow condition (no mass escapes),

$$w\left(x, 0\right) = w\left(x, H\right) = 0, \tag{11}$$

and a no slip boundary at the bottom of the domain means the horizontal velocity on the bottom boundary is also zero:

$$u\left(x, 0\right) = 0. \tag{12}$$

The top boundary is free-slip with the horizontal velocity set to geostrophic; since the derivatives along the front are zero, this leads the horizontal velocity on the top boundary to also be zero:

$$u\left(x, H\right) = -\frac{g}{f}\frac{\partial v\left(x, H\right)}{\partial y} = 0. \tag{13}$$

Since w is zero along the top and bottom, ψ must also be zero here:

$$\psi\left(x, 0\right) = \psi\left(x, H\right) = 0. \tag{14}$$

Boundary conditions for η come from the Thom formulation (Weinan and Lu, 1996):

$$\eta\left(x, 0\right) = \frac{2}{\Delta z^2}\psi\left(x, 0\right), \tag{15}$$

$$\eta\left(x, H\right) = \frac{2}{\Delta z^2}\psi\left(x, H\right). \tag{16}$$

Other variables are all set such that their vertical derivatives are zero on the boundaries (the no flux condition), apart from θ_l on the bottom boundary which is used to provide a heating forcing to the model:

$$\frac{\partial \theta_l\left(x, 0, t\right)}{\partial z} = f(x, 0, t). \tag{17}$$

All code has been written in MATLAB.

3 Advection scheme

Flux limiters (and slope limiters, which have the same mathematical form) work by limiting the gradient of numerical advection where it encounters shocks or discontinuities. Such schemes will typically use a high-order solution where the advected field is smooth, but where the gradient of this field changes, this high-order flux is blended with a lower-order one which prevents numerical oscillations being introduced. There are many forms for the flux-blending function, usually denoted ϕ (see for instance Sweby (1984)). A common example, and the function used throughout this work, is the minmod function:

$$\text{minmod}\,(a,b) = \frac{1}{2}\left[\text{sgn}\,(a) + \text{sgn}\,(b)\right] \cdot \min\left(|a|,|b|\right). \tag{18}$$

In this section, two flux-limiter advection schemes are introduced. For simplicity, the schemes are described for the 1D advection case where the schemes solve the PDE,

$$\frac{\partial q_j}{\partial t} + \frac{\partial f\,(q_j)}{\partial x} = 0, \tag{19}$$

$q_j = q\,(x_j,t) = q\,(j\Delta x,t)$ where Δx is the horizontal grid spacing. Similarly, in the vertical, $q_k = q\,(z_k,t) = q\,(k\Delta z,t)$ where Δz is the vertical grid spacing.

3.1 Simple flux-limiting scheme

A simple flux-limiting scheme, similar to that described in Gustafsson et al. (1995), has been coded by R. Hogan. The output is weighted between a central difference $\left(f^{high}\right)$ and Euler upwind scheme $\left(f^{low}\right)$ in the presence of changes in gradients. Written in semi-discrete form, equation 19 is

$$\frac{\partial q_j}{\partial t} = \frac{f_{j-1/2} - f_{j+1/2}}{\Delta x}. \tag{20}$$

Firstly, the advection fluxes are calculated for the half-points between each j, with the points used for the Euler upwind scheme depending on the direction of the wind u at point $j+1/2$:

$$f^{high}_{j+1/2} = u_{j+1/2}\left(q_{j+1} - q_{j-1}\right)/2, \tag{21}$$

$$f^{low}_{j+1/2,u>0} = u_{j+1/2}\,q_j, \tag{22}$$

$$f^{low}_{j+1/2,u<0} = u_{j+1/2}\,q_{j+1}. \tag{23}$$

The fluxes for the negative half-point are calculated in the equiavlent way. Then, ratios of values at successive points are calculated, also depending on the direction of the wind at point $j+1/2$:

$$r_{u>0} = \frac{q_j - q_{j-1}}{q_{j+1} - q_j}, \tag{24}$$

$$r_{u<0} = \frac{q_{j+2} - q_{j+1}}{q_{j+1} - q_j}. \tag{25}$$

This ratio is used to evaluate the flux limiting function phi,

$$\phi\,(r) = \text{minmod}\,(r,1)\,, \tag{26}$$

then this function is used to blend the high- and low-order advection fluxes:

$$f_{final} = f_{low} - \phi\,(r)\left(f_{low} - f_{high}\right). \tag{27}$$

This scheme is referred to as the 'RH' scheme, and is TVD, 2nd order for slowly-varying fields and 1st order when the gradient changes sign.

3.2 The Kurganov-Tadmor scheme

A more sophisticated flux limiting scheme is presented in Kurganov and Tadmor (2000): the 'KT' scheme. They introduced a family of central difference schemes that are 2nd order, TVD, semi- or fully-discrete and extendable to two dimensions and parabolic equations. For now, we consider the 1D semi-discrete scheme:

$$\frac{d}{dt}q_j(t) = -\frac{\left[f\left(q^+_{j+1/2}(t)\right)+f\left(q^-_{j+1/2}(t)\right)\right]-\left[f\left(q^+_{j-1/2}(t)\right)+f\left(q^-_{j-1/2}(t)\right)\right]}{2\Delta x} + \frac{1}{2\Delta x}\left\{a_{j+1/2}(t)\left[q^+_{j+1/2}(t)-q^-_{j+1/2}(t)\right]-a_{j-1/2}(t)\left[q^+_{j-1/2}(t)-q^-_{j-1/2}(t)\right]\right\}. \quad (28)$$

The half-points are defined by extrapolation via Taylor series:

$$q^+_{j+1/2}(t) = q_{j+1}(t) - \frac{\Delta x}{2}(q_x)_{j+1}(t), \quad (29)$$

$$q^-_{j+1/2}(t) = q_j(t) + \frac{\Delta x}{2}(q_x)_j(t), \quad (30)$$

and similarly for the negative half-points. The local speed a is defined via the spectral radius ρ of the Jacobian:

$$a_{j+1/2} = \max\left\{\rho\left[\frac{\partial f}{\partial q}\left(q^-_{j+1/2}\right)\right], \rho\left[\frac{\partial f}{\partial q}\left(q^+_{j+1/2}\right)\right]\right\}. \quad (31)$$

It is important to note that this is a local speed, i.e. the absolute value of the velocity, as this applies upwinding in the second term on the right hand side of equation 28.

The key part of this scheme in achieving the accuracy and TVD properties listed above is the choice of the numerical derivative q_x. Kurganov and Tadmor suggest the minmod limiter, which we use here in the form:

$$(q_x)_j = \text{minmod}\left(\frac{q_j - q_{j-1}}{\Delta x}, \frac{q_{j+1}-q_j}{\Delta x}\right). \quad (32)$$

The equivalence of this scheme to the flux-limiting schemes using the function ϕ can be seen more easily if the scheme is written in conservative form:

$$\frac{d}{dt}q_j(t) = -\frac{H_{j+1/2}(t) - H_{j-1/2}(t)}{\Delta x} \quad (33)$$

$$H_{j+1/2}(t) = \frac{f\left(q^+_{j+1/2}(t)\right)+f\left(q^-_{j+1/2}(t)\right)}{2} - \frac{a_{j+1/2}(t)}{2}\left[q^+_{j+1/2}(t)-q^-_{j+1/2}(t)\right] \quad (34)$$

$$H_{j-1/2}(t) = \frac{f\left(q^+_{j-1/2}(t)\right)+f\left(q^-_{j-1/2}(t)\right)}{2} - \frac{a_{j-1/2}(t)}{2}\left[q^+_{j-1/2}(t)-q^-_{j-1/2}(t)\right] \quad (35)$$

where the half-points are now defined:

$$q^+_{j+1/2}(t) = q_{j+1}(t) - \frac{1}{2}\phi_{j+1}(r)(q_{j+2}-q_{j+1}), \quad (36)$$

$$q^-_{j+1/2}(t) = q_j(t) + \frac{1}{2}\phi_j(r)(q_{j+1}-q_j), \quad (37)$$

and

$$r = \frac{q - q_{j-1}}{q_{j+1}-q_j}. \quad (38)$$

It is simple to show that for linear advection, in the limit $\phi = 1$ the scheme is a central difference, while for $\phi = 0$ the scheme is Euler upwind.

4 Scheme testing

4.1 1D convergence and stability testing

Both the above schemes have been tested for their convergence rates and stability for the 1D nonlinear inviscid Burger's equation:

$$\frac{\partial q}{\partial t} + q\frac{\partial q}{\partial x} = 0 \tag{39}$$

$$q(x,0) = \sin(x) \tag{40}$$

Both schemes use the 4th order Runge-Kutta scheme for timestepping.

For convergence testing, the schemes are run for one timestep Δt which is kept constant over a range of Δx. Δt must be small enough that the errors introduced by the timestepper are smaller than those introduced by the spatial advection scheme. Convergence properties are demonstrated by calculating the error after one timestep and plotting this error with respect to the gridspacing. On a log scale, the result should be a straight line with the gradient representing the rate of convergence of the scheme. The RMS was chosen as the error norm, as the errors are normalised by the length of the model vector, which changes with gridspacing.

The results for the Burger's equation are shown in figure 2. Both schemes converge at the expected rate of 1.5, since for this sinusoidal function the schemes are an equal combination of 2nd and 1st order components. The results of the convergence test for the limits $\phi = 0$ and $\phi = 1$ are also shown in figure 2, compared to the high-order and low-order fluxes returned from the RH scheme. These plots show that both schemes are converging as expected: 2nd order for the central difference and 1st order for the Euler upwind.

Each scheme has also been run for a longer time to check its stability. Figure 3 shows the result of running the KT and RH schemes over 150 timesteps. Both schemes are stable.

4.2 Extension to 2D and the real model equations

To advect a 2D field, the schemes are applied in each direction consecutively. For the KT scheme this is written as:

$$\frac{d}{dt}q_{j,k}(t) = -\frac{H^x_{j+1/2,k}(t) - H^x_{j-1/2,k}(t)}{\Delta x} - \frac{H^z_{j,k+1/2}(t) - H^z_{j,k-1/2}(t)}{\Delta z}, \tag{41}$$

$$H^x_{j+1/2,k}(t) = \frac{f\left(q^+_{j+1/2,k}(t)\right) + f\left(q^-_{j+1/2,k}(t)\right)}{2} - \frac{a^x_{j+1/2,k}(t)}{2}\left[q^+_{j+1/2,k}(t) - q^-_{j+1/2,k}(t)\right], \tag{42}$$

$$H^z_{j,k+1/2}(t) = \frac{f\left(q^+_{j,k+1/2}(t)\right) + f\left(q^-_{j,k+1/2}(t)\right)}{2} - \frac{a^z_{j,k+1/2}(t)}{2}\left[q^+_{j,k+1/2}(t) - q^-_{j,k+1/2}(t)\right]. \tag{43}$$

The fluxes for the negative half-points are constructed in an equivalent way.

When the KT scheme was implemented in the full model, the scheme was found to become unstable when advecting one of the fields, the liquid water potential temperature (θ_l). Figure 4 shows the θ_l field, the x- and z-direction components of the advection term at the 'wiggle' point after one call of the advection scheme, and the advecting velocities u and w. The θ_l field is sinusoidal in x, and instabilities are generated where the derivative of this field is zero, i.e. the centre and boundary of the x-domain.

The cause of the instability is shown in figure 5: at the unstable points, the term for advection in the z-direction is smooth, while in the x-direction the term is kinked. The source of the kink is shown in figure 6. The flux limiter ϕ mixes the contribution of the gradient ahead of the point with that from behind (eqns 36 and 37), and, by construction, the value of ϕ goes to zero when the gradient of

the advected field is zero, even if it is smooth. At this turning point, the output jumps from one curve to the other, generating the kinked output. Different functions have been tried for ϕ but the same behaviour is observed. It is the interaction of the advection in the two directions at this point that leads to the unstable behaviour. In this case, the x and z parts of the advection should sum to zero, since both $\partial\theta_l/\partial x$ and w are zero at this point. The numerical artifact in the x-component means that the two do not quite sum to zero, and this discrepancy is then magnified over time.

If the field is advected purely in the x direction, the 'kink' is seen, but the size of the instability does not grow with time. This is also the case for the RH scheme: a similar kink is seen in the x-component of the advection, but this kink is not amplified when the advection components are combined in the full model.

5 Discussion and conclusions

The instability encountered when extending the KT scheme to 2D, has not been discussed in the literature. A somewhat analogous situation was described by Bermudez and Vazquez (1994) with respect to the balancing of source and flux terms in a steady state solution to the shallow water equations. Bermudez and Vazquez show that if the flux is approximated by an upwinded term, the source term must also be approximated in an appropriate way, to ensure the terms balance numerically as well as analytically.

A resolution to this problem has not been found. The moist convection model therefore uses the simpler RH scheme for advection.

References

A. Bermudez and M.E. Vazquez. Upwind methods for hyperbolic conservation laws with source terms. *Computers Fluids*, 23:1049–1071, 1994.

D. Clifford. Documentation for the moist version of the MIDAS model. Technical report, National Centre for Earth Observation, University of Reading, 2011. URL `http://www.met.reading.ac.uk/~vx900751/reasearch/model_documentation.pdf`.

B. Gustafsson, H.-O. Kreiss, and J. Oliger. *Time dependent problems and difference methods*. Wiley-Interscience, 1995.

G.J. Haltiner and R.T. Williams. *Numerical prediction and dynamic meteorology*. Wiley, 1980.

A. Kurganov and E. Tadmor. New high-resolution central schemes for nonlinear conservation laws and convection-diffusion equations. *Journal of Computational Physics*, 160:241–282, 2000.

C.J. Morcrette and K.A. Browning. Formation and release of symmetric instability following Delta-M adjustment. *Quarterly Journal of the Royal Meteorological Society*, 132:1073–1089, 2006.

J.L. Peterson and G.W. Hammett. A comparison of numerical methods for simulating edge plasmas (poster). In *EU-US TTF Workshop, Copenhagen, Denmark*, 2008.

J. Sun and A. Crook. Dynamical and microphysical retrieval from Doppler radar observations using a cloud model and its adjoint. part I: model development and simulated data experiments. *Journal of the Atmospheric Sciences*, 54:1642–1661, 1997.

H. Sundqvist. A parameterization scheme for non-convective condensation including prediction of sloud water content. *Quarterly Journal of the Royal Meteorological Society*, 104:677–690, 1978.

P. Sweby. High resolution schemes using flux-limiters for hyperbolic conservation laws. *SIAM J. Num. Anal.*, 21:995–1011, 1984.

G.J. Tripoli and W.R. Cotton. The use of ice-liquid water potential temperature as a thermodynamic variable in deep atmospheric models. *Monthly Weather Review*, 109:1094–1102, 1981.

E. Weinan and J.-G. Lu. Vorticity boundary condition and related issues for finite difference schemes. *Journal of Computational Physics*, 124:368–382, 1996.

D.R. Wilson and S.P. Ballard. A microphysically based precipitation scheme for the UK Meteorological Office Unified Model. *Quarterly Journal of the Royal Meteorological Society*, 125:1607–1636, 1999.

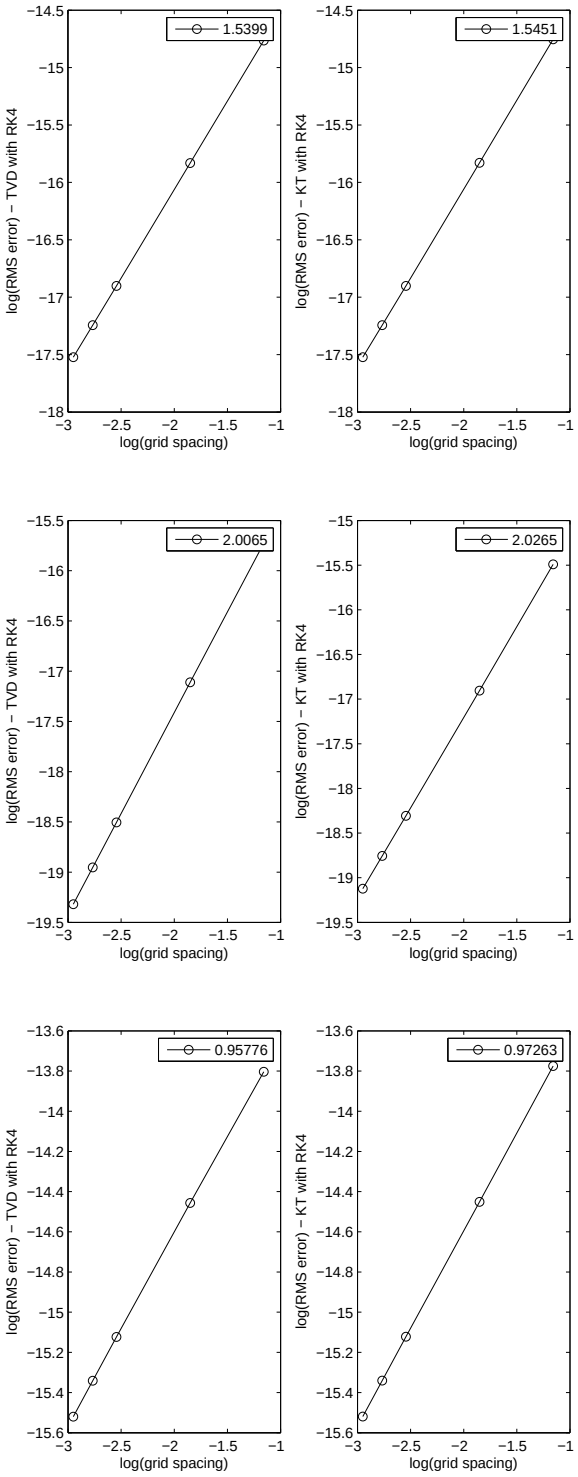

Figure 2: Spatial convergence for the RH (left) and KT (right) schemes. The top rows shows results when using the minmod function for ϕ, the middle row is for KT using $\phi = 0$, RH using low-order flux, and the bottom row shows KT with $\phi = 1$, and RH with the high-order flux. The gradient of a linear fit in each case is shown in the box at the top-right of each subfigure. In all cases the timestep was 10^{-6}s.

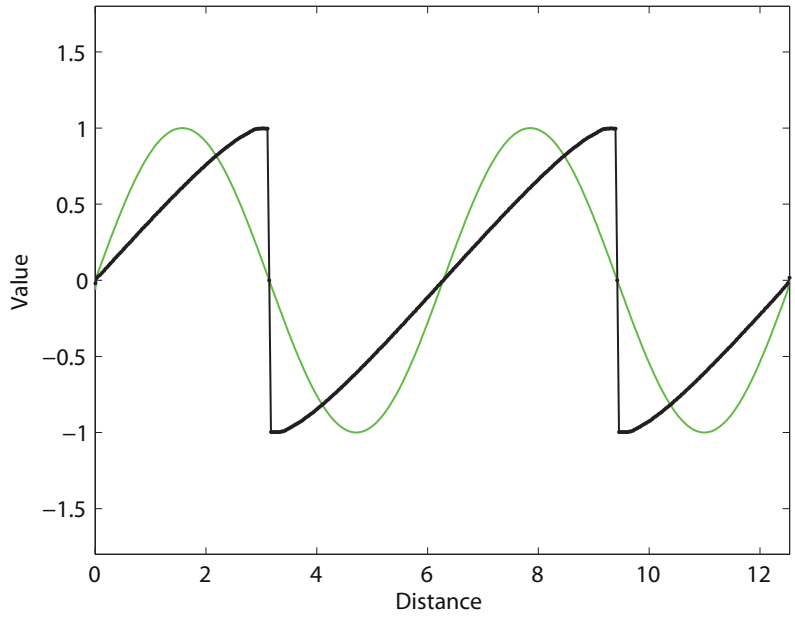

(a) RH

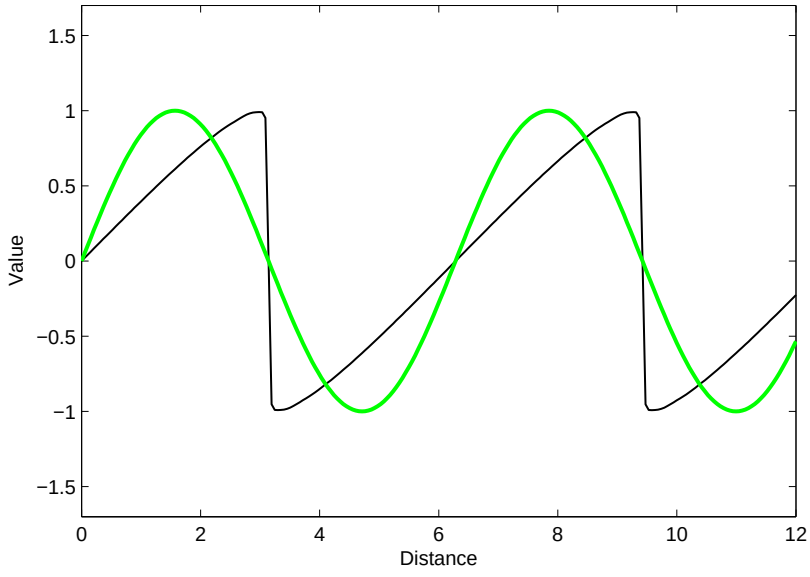

(b) KT

Figure 3: Result of running the Burgers equation with the RH (a) and KT (b) schemes over 150 timesteps with $\Delta t = 0.01$. The initial condition is shown in green and the final values in black.

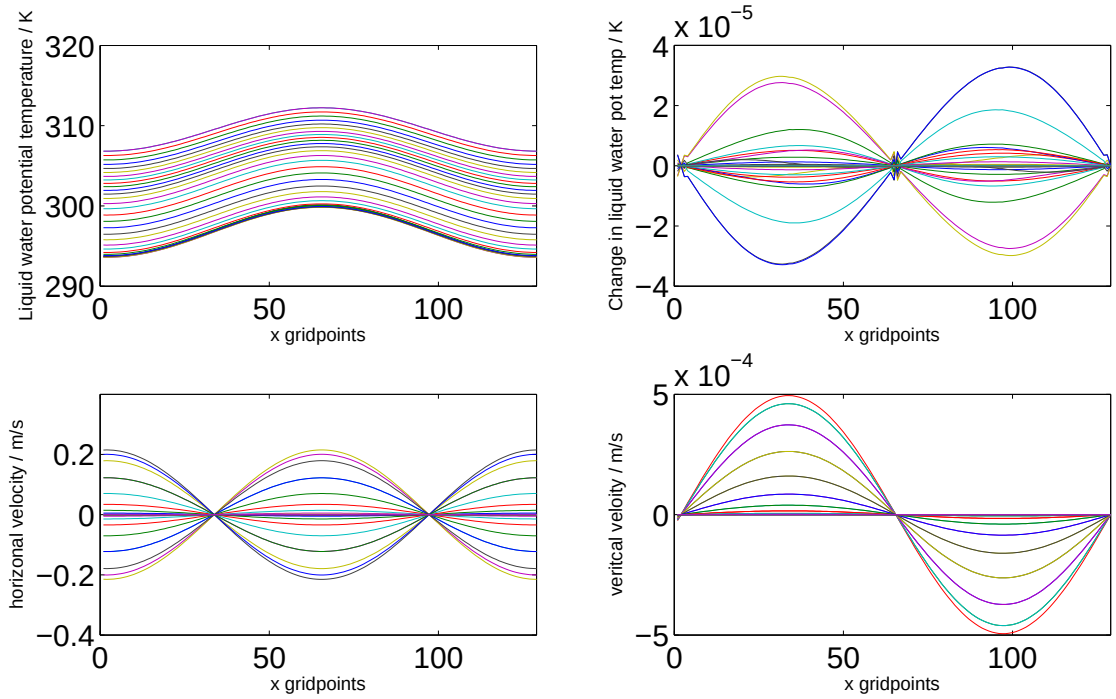

Figure 4: Advection of liquid water potential temperature θ_l, as a function of horizontal (x) gridpoint; the different colours show each of the 33 vertical model levels. Top left: initial θ_l field. Top right: output from call of advection scheme. Bottom left: horizontal wind field u. Bottom right: Vertical wind field w.

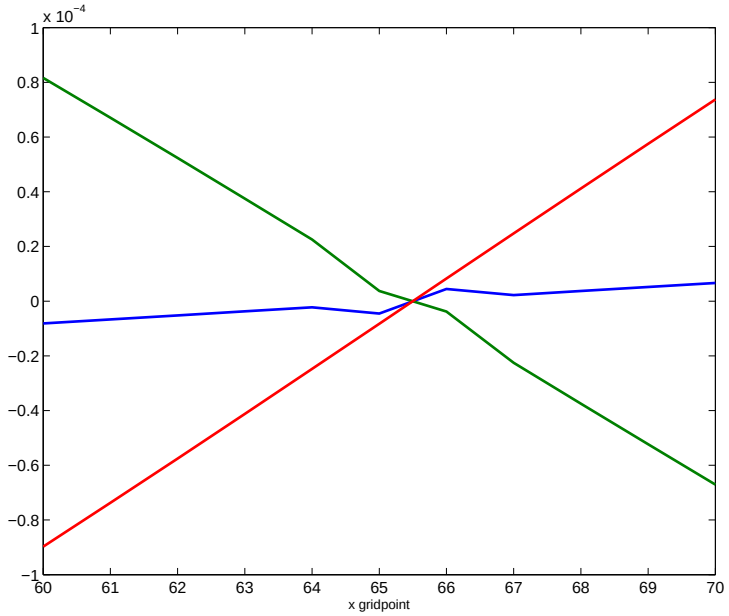

Figure 5: A close-up of the region where the 'wiggle' is occurring in the potential temperature advection increment. Shown is the advection term $u\frac{\partial \theta_l}{\partial x} + w\frac{\partial \theta_l}{\partial z}$ (blue), the x-component of the advection $u\frac{\partial \theta_l}{\partial x}$ (green) and the z-component $w\frac{\partial \theta_l}{\partial z}$(red).

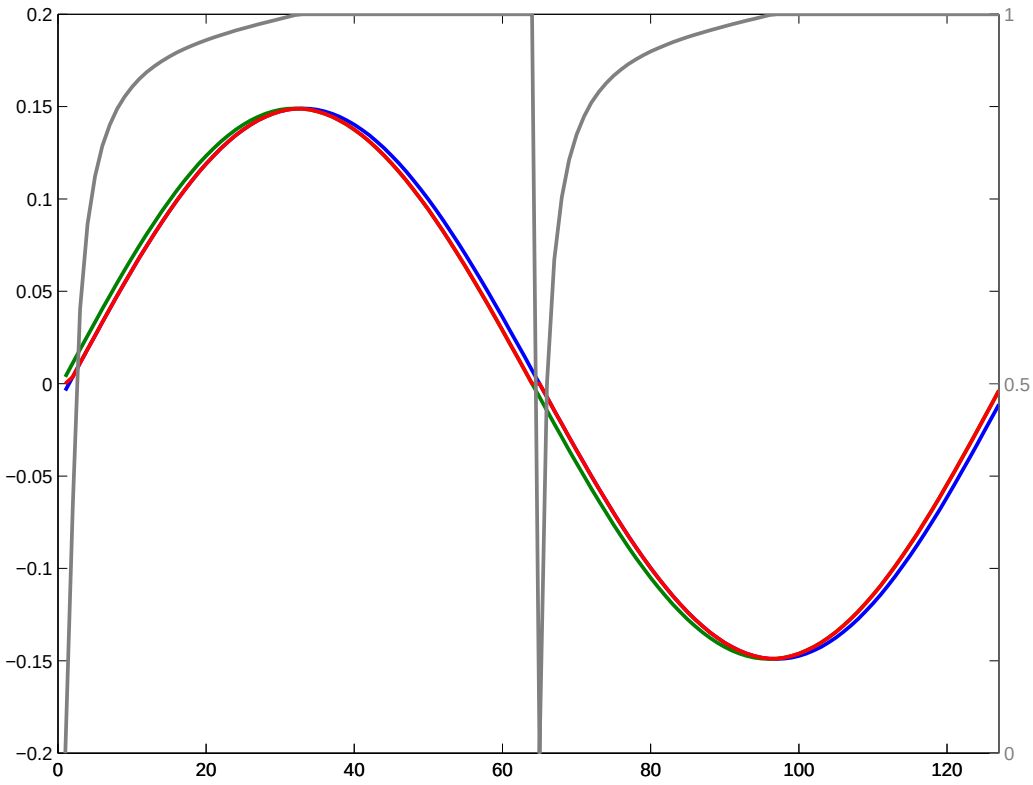

Figure 6: Example of the estimation of one of the half-point terms in the KT scheme (equation 37) applied to the potential temperature field in the x-direction. Shown is $(q_j - q_{j-1})$ in blue and $(q_{j+1} - q_j)$ in green. The flux-limiting function ϕ is shown in grey, and the result of applying ϕ to the forward difference $(q_{j+1} - q_j)$ in red, the last term in equation 37. A kink in the red curve can be seen at the centre of the domain, and at the boundaries, where $\phi = 0$.